*Acta Cryst.* (1982). A38, 177–186



# Structural Studies on *A*-Cation-Deficient Perovskite-Related Phases. I. $ThNb_4O_{12}$. Thorium/Vacancy Ordering in Slow-Cooled Samples

BY M. A. ALARIO-FRANCO

*Departamento de Quimica Inorgánica, Facultad de Ciencias Quimicas, Universidad Complutense, Madrid-3, Spain*

I. E. GREY,* J. C. JOUBERT AND H. VINCENT

*Laboratoire de Cristallographie, CNRS, 166 X, 38042 Grenoble Cedex, France*

AND M. LABEAU

*Institut National Polytechnique de Grenoble, Laboratoire de Génie Physique, BP 46, 38042-St Martin d'Heres, France*

(*Received* 11 *June* 1980; *accepted* 7 *July* 1981)

## Abstract

The *A*-cation-deficient perovskite, $Th_{0.25}NbO_3$, *i.e.* $ThNb_4O_{12}$, when slowly cooled from the melt, presents an interesting hierarchy of ordering phenomena. The associated diffraction effects have been studied with electron microscopy/diffraction and X-ray diffraction techniques. Three main types of ordering processes occur, with different degrees of long-range order. A primary ordering of thorium atoms into alternate $(001)_p$ planes of *A*-cation sites (cell $a_p \times b_p \times 2c_p$, *P4/mmm*) exhibits well-established long-range ordering. A secondary ordering of thorium atoms within the $(001)_p$ planes (cell $3\sqrt{2}a_p \times \sqrt{2}b_p \times 4c_p$, *Immm*) is short range in nature and gives rise to superlattice reflections in the form of diffuse rods directed along $g(110)_p$ and $g(\bar{1}10)_p$. The length of the rods corresponds to correlation lengths of only 20–30 Å between $\{110\}_p$ planes of thorium atoms, and the thorium/vacancy ordering is adequately described by a sinusoidal modulation model, with accompanying modulated displacements of niobium and oxygen atoms. Thirdly, a system of octahedral tilts about $[110]_p$ or $[\bar{1}10]_p$ axes is described by a cell $\sqrt{2}a_p \times \sqrt{2}b_p \times 2c_p$, *Pmam*. Independent models for thorium/vacancy ordering and octahedral tilts have been refined with the intensities of the corresponding groups of satellites measured from precession photographs. The complete model for $ThNb_4O_{12}$ can be described in the unit cell $3\sqrt{2}a_p \times \sqrt{2}b_p \times 4c_p$, *P2mm*. The superlattice reflections arising from the octahedral tilts are split into groups of four satellites in the form of crosses, owing to microdomain formation in $ThNb_4O_{12}$, with domain boundaries parallel to $(100)_p$ and $(010)_p$ and with average widths of ~25 Å.

## 1. Introduction

The existence of new 1:2 mixed oxides in the systems $AO_2$–$M_2O_5$, $A$ = U, Th, Ce, $M$ = Nb, Ta, was first reported by Kovba & Trunov (1962). They observed that the structures of the $AM_4O_{12}$ phases were all closely related to that of perovskite, and noted the presence of extra lines in the powder patterns which could be indexed with tetragonal superlattices. It appeared that the superstructures were different for the niobates and tantalates; for the former the $c_t$† axis was twice that of the cubic perovskite subcell, whereas, for the latter, the $a_p$ and $b_p$ axes were doubled. In a later paper, Trunov & Kovba (1966) reported the structure determination for one of the niobates, $ThNb_4O_{12}$, in space group *P4/mmm*. It comprised a perovskite-like framework of corner-shared $[NbO_6]$ octahedra with thorium atoms ordered into the cuboctahedral sites in *alternate* (001) layers along the $c_t$ axis; *i.e.* the (001) layers were alternately empty and half-filled. No evidence was presented for ordering of the thoriums within the half-filled layers. In the unit cell of Trunov & Kovba the only possibility was a statistical occupancy of half of the cuboctahedrons by thorium atoms. Keller (1965) reported that the superlattice for $ThNb_4O_{12}$ had

* Permanent address: CSIRO, Division of Mineral Chemistry, PO Box 124, Port Melbourne, Victoria 3207, Australia.

† Throughout this paper, subscript $p$ refers to the simple cubic perovskite aristotype and subscript $t$ refers to a tetragonal superstructure with $c_t = 2c_p$.

0567-7394/82/020177-10$01.00

$a_p$, $b_p$ and $c_p$ axes doubled. Although he did not discuss possible structural models, the larger unit cell clearly allowed for an ordering of thorium atoms within the half-filled (001) layers. Most recently the structure and properties of $ThNb_4O_{12}$ have been studied by Labeau & Joubert (1978). Their single-crystal X-ray studies confirmed the tetragonal cell found by Kovba & Trunov (1966); no evidence was found for the doubling of the $a_p$ and $b_p$ axes found by Keller (1965). However, as mentioned above, it was not possible to order the thorium atoms in the (001) half-filled layers with the smaller cell.

To resolve the problem of $A$-cation ordering in $ThNb_4O_{12}$ and related $A$-deficient perovskites we have carried out electron microscopy/diffraction studies which have revealed extra, diffuse diffraction effects associated with local $A$-cation-vacancy ordering. The electron diffraction studies have been complemented with long-exposure X-ray diffraction studies (precession method) to give quantitative intensity distributions. For $ThNb_4O_{12}$, quite different ordering patterns are observed for samples quenched or slowly cooled from near the melting point. For the former, thorium/vacancy ordering results in a doubling of all three perovskite subcell axes, as reported by Keller (1965), whereas for the latter a sinusoidal modulation model for the distribution of thorium atoms in a unit cell $3\sqrt{2}a_p \times \sqrt{2}b_p \times 4c_p$ gives a satisfactory explanation of the observed diffraction effects. The density modulation is accompanied by substantial displacements of the surrounding niobium atoms and large tilts of the octahedral framework. Both quenched and slowly cooled samples display periodic microdomain textures.

In this paper, we present an analysis of the electron and X-ray diffraction data for the slow-cooled sample of $ThNb_4O_{12}$ in the approximation of a single-domain model. The microdomain nature of the structures for slow-cooled and quenched $ThNb_4O_{12}$ and the structural modifications occurring across the domain boundaries will be presented in a subsequent publication (part II).

## 2. Experimental

Samples of $ThNb_4O_{12}$ were prepared by reacting mixtures of $Nb_2O_5$ and either $ThO_2.2H_2O$ or $ThO_2$ in air at temperatures just above 1661 K, the congruent melting point for the compound (Keller, 1965), for periods of 15 to 24 h then cooling the sample at 2 K $h^{-1}$ to 1173 K, at which point the furnace was switched off and the sample allowed to cool to ambient temperature (in several hours). Phase purity was checked by powder X-ray diffraction, with a Guinier focusing camera with Fe $K\alpha$ radiation. Refined lattice parameters have been previously published (Labeau & Joubert, 1978).

Single-crystal diffraction patterns were obtained by the precession method. Very long exposure times, 200–700 h were required to register clearly the diffuse diffraction effects associated with thorium/vacancy ordering and niobium/oxygen displacements. The intensities of the weak satellite reflections were visually estimated by comparison with a calibrated strip of intensities. Even for films exposed for >500 h, the intensities of the strongest satellites were not higher than 7 or 8 relative to the scale 1 to 20 on the calibrated strip and so the measured intensities have high associated errors, at least ±20% and generally higher for the weaker reflections.

Electron diffraction/microscopy studies were carried out with a Siemen's Elmiskop-102 electron microscope, operated at 100 kV and fitted with a double-tilting goniometer stage, allowing tilts of ±45° around both axes. Samples for study were crushed in an agate mortar and suspended in $n$-butanol, then transferred to holey carbon-coated copper grids.

## 3. Observations

### 3.1. *Electron diffraction results*

A $[010]_p$ zone diffraction pattern, Fig. 1(*a*), shows a doubling of $c_p$ but no doubling of $a_p$, consistent with the early observations of Kovba & Trunov (1962). Similarly, a $[001]_p$ zone diffraction pattern, Fig. 1(*b*), shows no extra reflections at $(\frac{1}{2}00)_p$ and $(0\frac{1}{2}0)_p$ as reported by Keller (1965). However, at $(\frac{1}{2}\frac{1}{2}0)_p$ and related positions, a cluster of four weak spots in the form of a cross is observed. The two arms of the cross are directed along $g(010)_p$ and $g(100)_p$ and a careful measurement of the separation between pairs of split spots, Fig. 1(*c*), indicates superperiods of $12 \times a_p$ and $12 \times b_p$. The pattern shown resembles those observed for alloys containing one-dimensional periodic antiphase boundaries, *e.g.* CuAu(II) (Ogawa, 1962). It will be seen below that the origin of the crosses is, however, different in this case. A $[\bar{1}10]_p$ zone diffraction pattern is shown in Fig. 1(*d*). Around each sharp reflection of the tetragonal cell ($a_t = a_p$, $c_t = 2c_p$) are arranged a group of four diffuse spots in an approximately square configuration. The positions of these satellites correspond to odd multiples of $\frac{1}{4}d^*(001)_p$ and $\frac{1}{6}d^*(110)_p$. An identical pattern is observed for the $[110]_p$ zone axis diffraction pattern. The intersection of the 'crosses' observed in Fig. 1(*b*) with the $[\bar{1}10]_p$ zone gives rise to the extra reflections seen at $(h/2,h/2,l/2)_p$, $h$ odd, $l$ odd and even in Fig. 1(*d*). Because of the slight curvature of the Ewald sphere, the $[\bar{1}10]_p$ zone intersects the arms of the crosses, thus giving rise to pairs of spots at high-$\theta$ values. An image corresponding to the diffraction pattern in Fig. 1(*d*) is shown in Fig. 1(*e*). White fringes parallel to $[334]_p$ and $[33\bar{4}]_p$ are resolved into alternate white and black blobs in different parts of the image. The separation of the white spots along [001] and [110]

is 4 × $d(001)_p$ (15·7 Å) and 6 × $d(110)_p$ (16·5 Å), consistent with the satellite periodicities observed in Fig. 1(*d*).

When the satellite reflections are viewed in sections approximately perpendicular to that shown in Fig. 1(*d*), it is seen that they are not discrete spots but rods of diffuse intensity, elongated along $g(\bar{1}10)_p$. For example, in Fig. 2(*a*), one set of ⟨110⟩ rods is observed in a $[11\bar{2}]_p$ diffraction pattern, whereas, in Fig. 2(*b*), two equivalent sets of ⟨110⟩ rods appear in a $[\bar{1}04]_p$ diffraction pattern. In Fig. 2(*c*) the diffraction pattern is tilted slightly off the $[001]_p$ zone around $[110]_p$ and diffuse rods along $g(110)_p$ and $g(\bar{1}10)_p$ are observed together with some 'crosses' which lie in the $[001]_p$ zone as shown in Fig. 1(*b*). In Fig. 3 we have combined the various observations to give a 3D representation of the reciprocal lattice. The two features discussed above are evident, *i.e.* (*a*) planar groups of four diffuse rods of intensity forming squares with sides parallel to $g(110)_p$ and $g(\bar{1}10)_p$ and (*b*) clusters of four spots in the form of

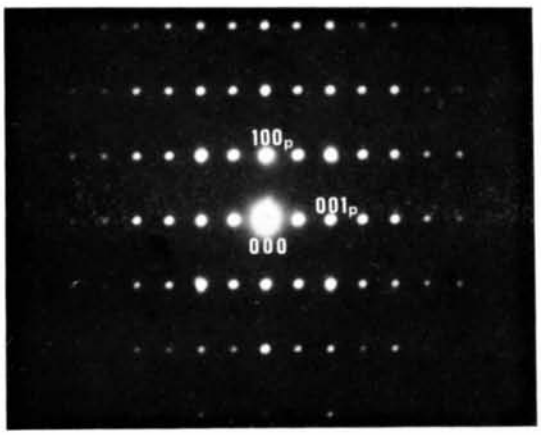


(*a*)

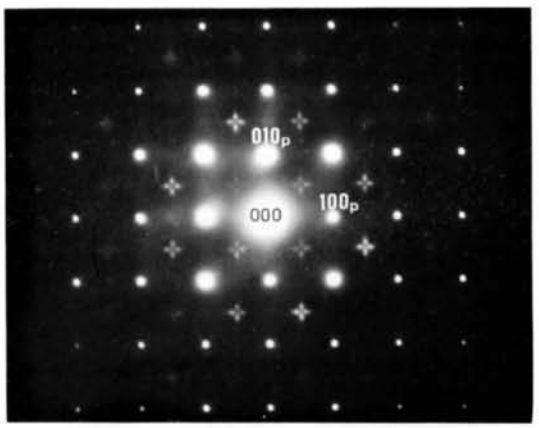


(*b*)

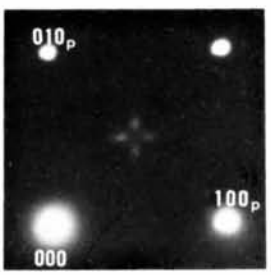


(*c*)

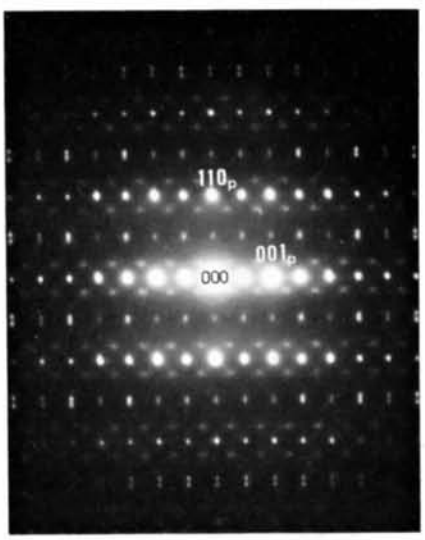


(*d*)

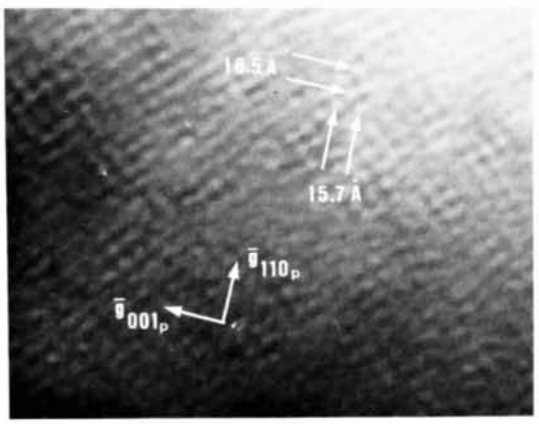


(*e*)

Fig. 1. Electron diffraction/microscopy patterns for $ThNb_4O_{12}$. (*a*) $[010]_p$ zone diffraction pattern, (*b*) $[000]_p$ zone diffraction pattern, (*c*) enlargement of part of (*b*), (*d*) $[\bar{1}10]$ zone diffraction pattern, (*e*) bright-field image corresponding to the $[\bar{1}10]_p$ diffraction pattern in (*d*).

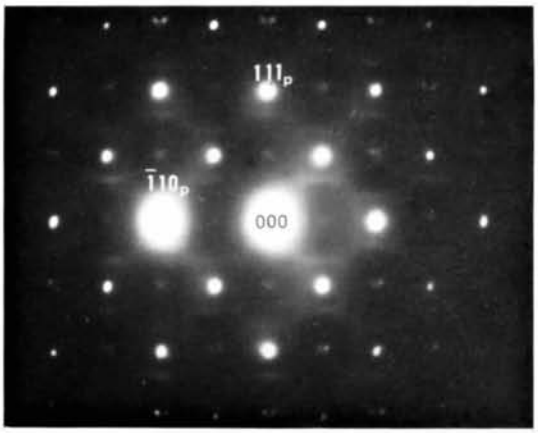


(*a*)

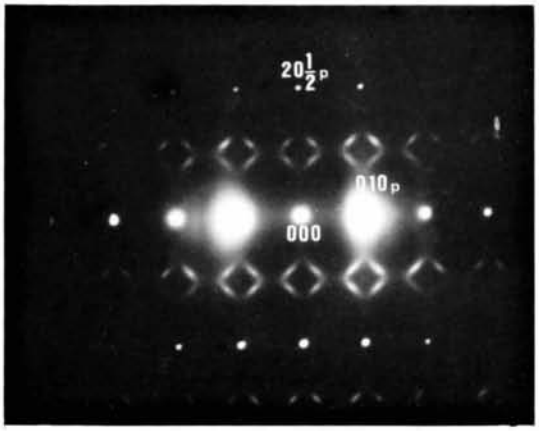


(*b*)

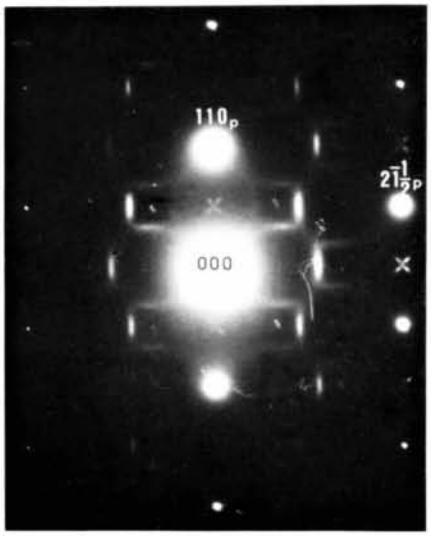


(*c*)

Fig. 2. Electron diffraction patterns displaying diffuse rod-like satellites due to thorium/vacancy ordering. (*a*) $[11\bar{2}]_p$ zone diffraction pattern showing one orientation of $\langle 110\rangle_p$ rods. (*b*) $[104]_p$ zone diffraction pattern showing two sets of $\langle 110\rangle_p$ rods. (*c*) Diffraction pattern is tilted slightly off the $[001]_p$ zone axis, to show both rods and 'crosses', *c.f.* Fig. 1(*b*).

crosses, with arms parallel to $g(100)_p$ and $g(010)_p$ and with the spots slightly elongated along these directions.

### 3.2. *X-ray diffraction results*

When long exposure times (200–700 h) were employed, precession photographs showed all the features observed in the electron diffraction patterns, but the true intensity distribution as shown by X-ray diffraction was significantly different. For example, Fig. 4(*a*) shows schematically the intensity distribution of satellite reflections for the $[\bar{1}10]_p$ zone of the slowly cooled sample (*cf.* the electron diffraction pattern in Fig. 1*d*). As in the case of electron diffraction, only first-order satellites are observed. However, in contrast to Fig. 1(*d*), where four equal-intensity satellites are observed around each subcell node, the precession photograph shows one, two, three or four satellites, with different intensities, around different subcell nodes. The pattern of satellite intensities repeats itself along successive rows parallel to $g(001)_p$, *i.e.* along rows $(11l)_p$, $(22l)_p$, *etc.* Reciprocal-lattice sections perpendicular to the $[\bar{1}10]_p$ zone diffraction pattern showed that the satellite reflections were in the form of diffuse rods, elongated along $g(\bar{1}10)_p$, and from the length of the rods a correlation length of about 25 Å is calculated. This may be compared with a value of about 20–25 Å, determined from the electron diffraction photographs.

Even exposures of hundreds of hours failed to reveal the 'crosses' at positions $(h/2,k/2,0)_p$ in $[001]_p$ zone precession photographs as was observed with electrons, Fig. 1(*b*). However, they were observed in upper-level photographs, centred around sub-cell nodes such as $(\frac{113}{222})_p$, $(\frac{117}{222})_p$, $(\frac{331}{222})_p$, $(\frac{335}{222})_p$, *i.e.* for odd multiples of the reciprocal-lattice vectors in a doubled perovskite unit cell, $2a_p \times 2b_p \times 2c_p$.

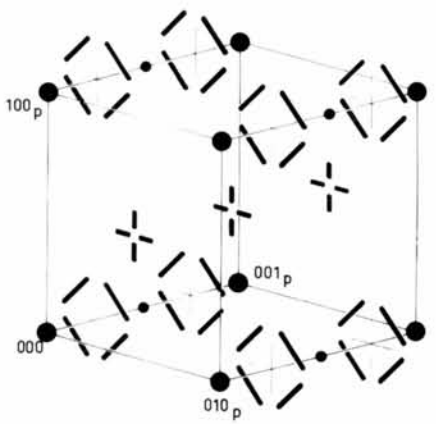


Fig. 3. Perspective drawing of the reciprocal lattice for $ThNb_4O_{12}$, showing diffuse diffraction effects in the form of both 'rods' and 'crosses' as they are observed to occur in electron diffraction patterns.

## 4. Structural model in a single-domain approximation

The observed splitting of the $(h/2,k/2,l/2)$ reflections into clusters of four satellites in the form of 'crosses', Fig. 1(*b*), suggests a microdomain structure for $ThNb_4O_{12}$, *cf.* similar observations for alloys (Ogawa, 1962). From measurements made on diffraction patterns such as that shown in Fig. 1(*c*) we find that the microdomain boundaries are parallel to $(100)_p$ and $(010)_p$ and with average periodicities of $12 \times a_p$ and $12 \times b_p$, respectively, corresponding to average domain widths of $6 \times a_p$, $6 \times b_p$, *i.e.* ~25 Å. Assuming a regular disposition of domains, a structure solution in a $12 \times a_p$, $12 \times b_p$, $4 \times c_p$ supercell is possible in principle and should explain all the essential features of the diffraction patterns. However, in practice, a direct structure solution was not possible in this large unit cell. In particular the number of observations to number of parameters was extremely unfavorable as only first-order satellites were observed around subcell nodes. Also, the derived model would be forced to have a perfectly regular domain arrangement and intra-domain ordering, which is not likely to occur in practice.

In an alternative approach we have first established a model for the ordering within an individual domain, by considering only one set of the $\langle 110 \rangle_p$ rod-like satellites and by replacing the 'crosses' of $\langle 100 \rangle_p$ satellites by discrete spots. It is clear from the appearance of these two groups of satellites that they have different structural origins and so, to a good approximation, the structural effects giving rise to the two types of satellites can be treated independently. The two sets of information may then be combined to give a complete model for ordering within a single domain. This approach is described below. In part II we consider modifications to the single-domain description which result from the introduction of microdomain boundaries parallel to $(100)_p$ and $(010)_p$.

### 4.1. *Analysis of rod-like satellites*

We interpreted the diffuse rod-like satellites as due essentially to ordering of thorium atoms and vacancies in the *A*-cation sites of the perovskite structure, although, to anticipate the results of this section, we found that to reproduce the observed intensity patterns it was necessary also to include significant displacements of the surrounding niobium and oxygen atoms.

The unit cell corresponding to the distribution of one set of rod-like satellites is orthorhombic, *I* centered, with axes given in relation to the perovskite subcell as

$$a = 3(a_p + b_p) = 16{\cdot}54 \text{ Å}$$

$$b = -a_p + b_p = 5{\cdot}513 \text{ Å}$$

$$c = 4c_p = 15{\cdot}70 \text{ Å}.$$

Apart from the body-centering condition, no systematic absences occurred for the satellite reflections and possible orthorhombic space groups are *Immm*, *Imm*2, *I*222 and $I2_12_12_1$. The fact that only first-order satellites were observed indicates that the distribution of scattering density due to thorium-vacancy ordering should be adequately described by a sinusoidal modulation.* As such a model is necessarily centrosymmetric, we used the space group *Immm*. With the limitation that the average thorium occupation of successive layers of *A*-cation sites, parallel to (001), is

* In a harmonic approximation, the superlattice periodicities need not be, and in general are not, simple integral multiples of the subcell parameters. In fact, we find for the related phase $LaNb_3O_9$ that $a = 3{\cdot}4\sqrt{2}a_p$. However, for $ThNb_4O_{12}$, as shown above, the superperiods were fortuitously integral multiples of the face-centered perovskite subcell, $(\sqrt{2}a_p, \sqrt{2}b_p, c_p)$.

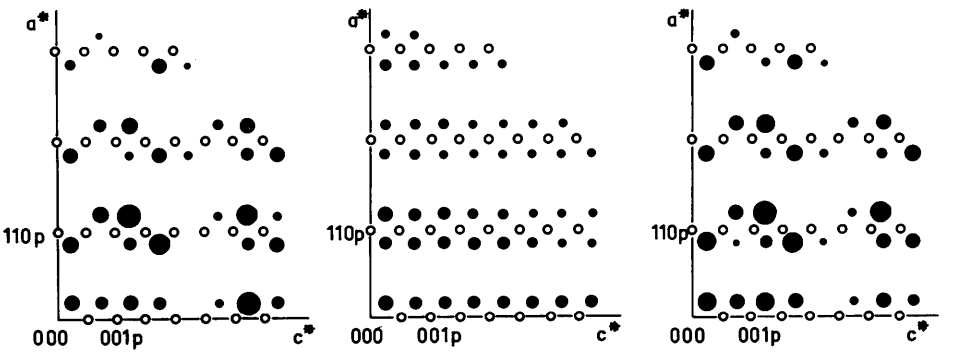


Fig. 4. Observed, (*a*), and calculated, (*b*) and (*c*), $F^2$ distributions for the rod-like superlattice reflections in the $[\bar{1}10]_p$ zone diffraction pattern. Observed intensities were measured from precession photographs and reduced to $F^2$ by applying Lp corrections. The area of the filled circles is proportional to $F^2$. The calculated pattern in (*b*) results from the sinusoidal modulation of thorium scattering density given in Table 1. In (*c*) displacements of niobium and oxygen atoms have been included in the calculation, see Table 1. The tetragonal subcell ($a_t = a_p$; $c_t = 2c_p$) reflections are shown schematically as small open circles.

alternately 0 and 0·5 (Trunov & Kovba, 1966), a unique model was obtained. It is described by a simple cosine function which was scaled to give a fully occupied thorium site at the origin of the unit cell and a total occupancy corresponding to the unit-cell formula $6(ThNb_4O_{12})$. The resulting thorium atom positions and site occupancies are given in Table 1. The calculated intensities (actually $F_c^2$) for this simple model are compared with the observed pattern for *h*0*l* reflections in Fig. 4(*b*). It is seen that although the correct geometrical disposition of satellites is obtained, the actual intensities are markedly different from those observed. It is evident that the density modulation is accompanied by an important displacement component. The agreement was improved somewhat by introducing thorium-atom displacements (see Table 1), but we were unable to reproduce the observed complex alternation of strong and weak satellites shown in Fig. 4(*a*). We next considered the possibility that niobium and/or oxygen displacements were contributing significantly to the intensities of the satellites. We determined the signs and approximate magnitudes of the *major* displacements by a simple qualitative procedure illustrated in Fig. 5. Fig. 5(*a*) shows the sign and qualitative magnitude [*i.e.* simply as observed (+, −) or unobserved (0)] of the structure factors for low-angle *h*0*l* reflections, resulting from the thorium-atom contributions only. Fig. 5(*c*) shows the observed distribution $F_o$ [where it is assumed that the thorium contribution is important enough that the *observed* reflections have the same sign of $F$ as in Fig. 5(*a*) – a reasonable assumption for the low-angle reflections depicted]. Then Fig. 5(*b*) represents qualitatively the sign and magnitude of the $F$'s (from displacement components), which have to be added to Fig. 5(a) to give the observed distribution in Fig. 5(*c*). The observed sequences of signs ± (+ − − +) for satellites 50*l* and 70*l*, $l$ = 1, 3, 5, 7 are reproduced by a simple cosine function, $\cos 2\pi lz$, $z = \pm(\frac{1}{8}, \frac{3}{8})$. As seen from Table 1, all the niobium atoms and some of the oxygens, O(1), O(2) and O(3), have $z$ coordinates of $\frac{1}{8}$ or $\frac{3}{8}$. The sequence of signs in the $a^*$ direction is more complex. The sign-generating function must be antisymmetric about $h = 6$, but have a value of zero at $h = 3$ (and $h$ = 2, 4). Obviously this cannot be reproduced by a single cosine function. The simplest possibility is a pair of functions $\cos 2\pi hx$ and $\cos 2\pi hx'$ which sum to zero at $h = 3$ and which reinforce at $h = 5$ and 7 (where the sum of the two functions at $h = 5$ and $h = 7$ must be of opposite sign). These conditions are met, and at the same time the values at $h = 5$ and 7 are at a maximum, for a pair of functions with $x \simeq 0{\cdot}20$ and $x' \simeq 0{\cdot}37$. The structure factor requirements of Fig. 5(*b*) are therefore met by the function $F = A \cos 2\pi l \times \frac{1}{8}(\cos 2\pi h \times 0{\cdot}20 + \cos 2\pi h \times 0{\cdot}37)$, *i.e.* from the contributions of a pair of displaced atoms at $(0{\cdot}20, y, \frac{1}{8})$

Table 1. *Sinusoidal model for thorium ordering in* $ThNb_4O_{12}$

Unit cell orthorhombic; *Immm*;
$a = 16{\cdot}551\ (4)$, $b = 5{\cdot}517\ (4)$, $c = 15{\cdot}716\ (4)$ Å.

| Atom | Occupation factor | Ideal coordinates | | Final coordinates | | |
|---|---|---|---|---|---|---|
| Th(1) | 1·0 | 2(*a*) | 000 | | | |
| Th(2) | 0·75 | 4(*f*) | $\frac{1}{3}0\frac{1}{2}$ | 0·325 (2) | 0 | $\frac{1}{2}$ |
| Th(3) | 0·25 | 4(*e*) | $\frac{1}{3}00$ | 0·320 (1) | 0 | 0 |
| Nb(1) | | 8(*m*) | $\frac{1}{6}0\frac{1}{8}$ | 0·181 (2) | 0 | 0·128 (2) |
| Nb(2) | | 8(*m*) | $\frac{1}{3}\frac{1}{2}\frac{1}{8}$ | 0·338 (2) | $\frac{1}{2}$ | 0·122 (2) |
| Nb(3) | | 4(*j*) | $\frac{1}{2}0\frac{3}{8}$ | $\frac{1}{2}$ | 0 | 0·359 (2) |
| Nb(4) | | 4(*j*) | $\frac{1}{2}0\frac{1}{8}$ | $\frac{1}{2}$ | 0 | 0·121 (2) |
| O(1) | | 16(*o*) | $\frac{1}{12}\frac{1}{4}\frac{1}{8}$ | | | |
| O(2) | | 16(*o*) | $\frac{1}{4}\frac{1}{4}\frac{1}{8}$ | | | |
| O(3) | | 16(*o*) | $\frac{5}{12}\frac{1}{4}\frac{1}{8}$ | | | |
| O(4) | | 2(*d*) | $0\frac{1}{2}0$ | | | |
| O(5) | | 4(*e*) | $\frac{1}{6}00$ | 0·150 | 0 | 0 |
| O(6) | | 4(*f*) | $\frac{1}{3}\frac{1}{2}0$ | 0·318 | $\frac{1}{2}$ | 0 |
| O(7) | | 2(*b*) | $\frac{1}{2}00$ | | | |
| O(8) | | 4(*j*) | $0\frac{1}{24}\frac{1}{4}$ | 0 | $\frac{1}{2}$ | 0·260 |
| O(9) | | 8(*m*) | $\frac{1}{6}0\frac{1}{4}$ | | | |

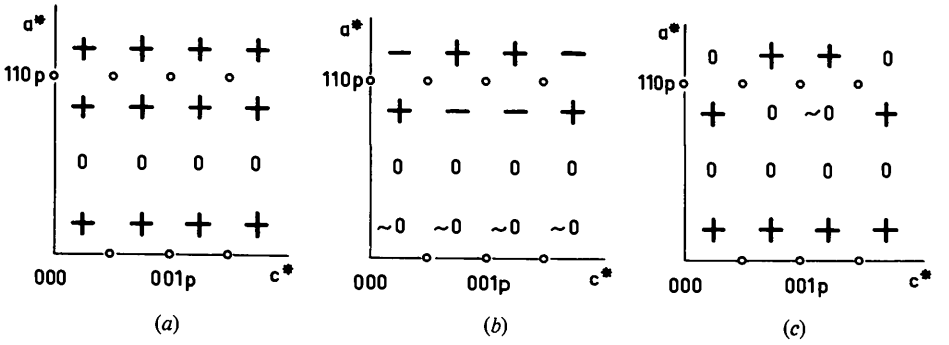


Fig. 5. Procedure for estimating the direction and approximate magnitude of the major displacement contributions to the intensities of superlattice reflections in the $[\bar{1}10]_p$ zone diffraction pattern. (*a*) Thorium atom contribution only. + and − signify the sign of the structure factor corresponding to an observed reflection, 0 signifies an unobserved reflection and ~0 indicates a very weak one. (*c*) Distribution of $F$'s corresponding to the observed pattern where it is assumed that the sign is determined by the thorium-atom contribution. (*b*) Required distribution of $F$'s due to atomic displacements, which when added to (*a*) gives the observed pattern (*c*).

and $(0{\cdot}37,y,\frac{1}{8})$. From Table 1, it is apparent that this corresponds to displacements along $a$ of niobium atoms Nb(1) and Nb(2). Although subsequent analysis showed that the displacements were overestimated in this simple approach, they were nevertheless in the correct sense and this allowed a least-squares refinement to proceed normally; the displacements of the remaining two niobium atoms were then determined from a difference Fourier map. A refinement of all cation positional parameters, a scale factor and an overall temperature factor converged at $R(F) = 0{\cdot}116$ for 95 observed $h0l$, $h1l$ and $h2l$ reflections. A difference Fourier map indicated displacements of some oxygen atoms and when these were included in the structure factor calculations the value of $R$ decreased slightly. However, owing to the relatively weak contributions from the oxygens, plus the poor quality of the intensity data, we were unable to refine the displaced oxygen atoms and their coordinates given in Table 1, taken from the Fourier map, must be considered with caution. The final $R$ factor was 0·104 for the 95 observed reflections and 0·156 for all 159 first-order satellites. We also confirmed that the calculated structure factors for all higher-order satellites were not greater than those of any of the observed first-order satellites. Calculated $F^2$ for the $h0l$ satellites are compared with the observed intensities in Fig. 4; in general the model closely reproduces the observed distribution of strong, weak and absent reflections.

A view of the structure along **b** is shown in Fig. 6, where the niobium displacements are indicated by the arrows. A close correspondence between the rhomb-shaped projection of columns of thorium atoms in Fig. 6 and the bright-field image shown in Fig. 1(*e*) is apparent. A complete through focal series of images taken from a $[\bar{1}10]_p$ diffraction photograph has confirmed in detail the features of the model shown in Fig. 6. Also apparent from the image shown in Fig. 1(*e*) is the very limited extent of single domains. When the direction of the thorium columns changes from $[\bar{1}10]_p$ to $[110]_p$, the rhombs of white spots are replaced by continuous lines. The results of the following sections have been anticipated in Fig. 6, by showing also the octahedral tilt system.

### 4.2. *Analysis of cross-like satellites*

If we replace the clusters of four spots forming the 'crosses' by discrete reflections we find that the indices for these reflections are all of the type $(h/2, k/2, l/2)_p$ with $h$, $k$ odd and $l$ even and odd, as shown in the electron diffraction pattern in Fig. 1(*d*). However, in X-ray diffraction patterns, the reflections with $l$ even were too weak to be observed and so a close approximation to the structure in a single domain may be described by reference to an $F$-centered double-perovskite cell, with $a = 2a_p$, $b = 2b_p$, $c = 2c_p$. By analogy with other perovskites which exhibit weak 'difference reflections' requiring a doubling of the perovskite subcell axes, we ascribed the satellites as due mainly to tilting of the octahedral framework. Glazer (1972) has reported a complete list of possible tilt systems in perovskites subject to the restriction that the superlattice periodicities are not more than twice the cubic subcell axes. Six of these tilt systems have $F$-centered cells with all axes doubled, as observed for $ThNb_4O_{12}$. Three correspond to three-tilt systems, two to two-tilt systems and one to a single-tilt system. A comparison of the observed intensity distribution of satellites for $ThNb_4O_{12}$ with those reported in the literature for perovskite exhibiting the different tilt systems gave closest qualitative agreement for a two-tilt system, as occurs for $PrAlO_3$ (Burbank, 1970), *i.e.* the tilt axes are parallel to one of the face diagonals $\langle 110\rangle_p$ of the perovskite subcell. Following Burbank (1970) we consider a body-centered unit cell rather than a face-centered cell, which is simply related to the perovskite subcell by

$$a' = a_p + b_p, \quad b' = -a_p + b_p, \quad c' = 2c_p,$$

where the cell orientation is the same as that for the cell defining the thorium ordering, § 4.1. The two cells are simply related by $a = 3a'$, $b = b'$, $c = 2c'$.

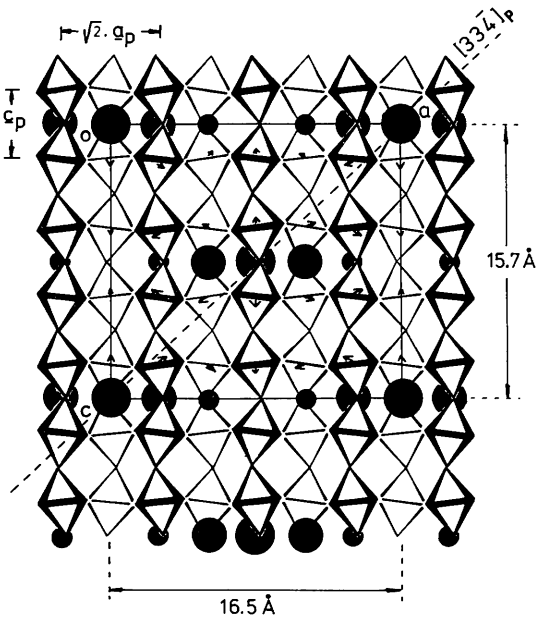


Fig. 6. Ordering of thorium atoms and vacancies in $ThNb_4O_{12}$. Projection along **b**, ($[\bar{1}10]_p$). Site occupations of 1, $\frac{3}{4}$ and $\frac{1}{4}$ for the thoriums are represented by large, medium and small filled circles, respectively. The direction and approximate magnitude of the niobium displacements is represented by the arrows. Heavy and lightly shaded octahedra are centered at $y = 0$ and $y = \frac{1}{2}$, respectively. The unit cell is outlined. The $[\bar{1}10]_p$ columns of thorium atoms are aligned in planes parallel to $(22\bar{3})_p$ and $(2\bar{2}3)_p$. These planes intersect the plane of the diagram along $[33\bar{4}]_p$ and $[334]_p$, shown by the dashed lines.

For small tilts about $\langle 110\rangle_p$ axes, the tilt system is $a_p^- a_p^- c_p^0$ in Glazer's notation (Glazer, 1972) and the corresponding space group is *Imam*, relative to the above axes $a'$, $b'$, $c'$. Structure factor calculations were carried out for combinations of oxygen displacements corresponding to various tilts of the octahedra about axes parallel to **a**′. Optimum values were quickly established, see Table 2, corresponding to a tilt angle of about 8°. This model gave an $R$ value of 0·25 for 14 observed satellites taken from $0kl$ and $2kl$ precession photographs. Some serious discrepancies existed; in particular, some unobserved reflections had $F_c$ values considerably higher than some of the observed $F_o$. We thus considered the possibility of thorium displacements. As previously discussed, the thorium atoms are ordered in alternate (001) planes and their distribution is not consistent with the *I*-centered space group describing the octahedral tilts. A number of possible models were considered in primitive subgroups of *Imam*. The most satisfactory model comprised displacement of thorium atoms by ~0·04 Å along **b**′. The complete model comprising octahedral tilts plus thorium displacements is described by the space group *Pmam*, a maximal isoclass subgroup of *Imam*. Of course, the actual thorium distribution, Table 1, cannot be described exactly in the smaller unit cell defining the octahedral tilts and so we carried out the structure factor calculations in the approximation of a statistical half-occupancy by thorium of the site 2(*e*) in *Pmam*. It was also necessary to correct for the contributions from domains oriented at 90° to one another. As seen from Table 2, the unit cell is metrically tetragonal and each observed reflection represents the superimposed contributions of *hkl* from one domain and *khl* from the second domain, rotated by 90° relative to the first. We assumed that no correlation existed between the domains and that there were equal contributions from the two orientations and so $F^2_{calc} = F(hkl)^2 + F(khl)^2$.

Refinement of the oxygen and thorium positions gave an $R(F)$ value of 0·10 for the 14 observed satellites on $0kl$ and $2kl$ levels (the $1kl$ level was exposed for only 300 h, *cf.* about 700 h exposures for $0kl$ and $2kl$ levels and the satellites were too weak to be measured with any precision). The value of $R(F)$ for all 42 $0kl$ and $2kl$ satellites was 0·13, with $F^2$(unobs) = $0{\cdot}5F^2_{min}$(calc). The atom coordinates and structure factors are given in Table 2.

The magnitudes of the atomic displacements obtained were a sensitive function of the scale factor used. Ideally the scale factor should be obtained from a refinement of the perovskite subcell reflections and held fixed during the refinement of the atomic positions, with the superlattice reflections. However, the very weak, diffuse nature of the superlattice reflections prevented an accurate determination of the geometrical factor which would enable the intensities of the subcell and superlattice reflections to be placed on the same scale, and so the magnitudes of the atomic shifts given in Table 2 must be considered with caution.

It is interesting to note that the octahedral tilt system $a_p^- a_p^- c_p^0$ causes the pseudocubic subcell parameters to have the relationships $a_p = b_p > c_p$, $\gamma \neq 90°$ whereas the observed relationships are quite different, $a_p = b_p < c_p$, $\gamma = 90°$. This difference may be explained if we take into account the effect of thorium/vacancy ordering on the unit-cell geometry. As seen from Fig. 6 there is an ordering of thorium atoms in planes parallel to $(223)_p$ and $(22\bar{3})_p$, which results in an effective separation of positive charge accompanied by an alternation of slabs of undersaturated and oversaturated oxygens. This will be compensated for by shortening and lengthening respectively of the $M$—O bonds. Because of the exponential form of the bond length–bond strength curves, the bond lengthening to produce a particular bond-strength change is greater than the corresponding shortening to produce the same (but of opposite sign) bond-strength change and so the overall effect is expansion perpendicular to $\{223\}_p$. This expansion can be divided into components along $[001]_p$ and $\langle 110\rangle_p$. The component along $[001]_p$ is the larger of the two and possibly explains why $c_p > a_p, b_p$.

If the expansion along $\langle 110\rangle_p$ is exactly matched by a contraction in the $\langle 110\rangle_p$ octahedral edges, brought about by octahedral tilting about axes parallel to the

Table 2. *Model for octahedral tilts in* $ThNb_4O_{12}$

Unit cell orthorhombic; *Pmam*;
$a' = 5{\cdot}517\ (1)$, $b' = 5{\cdot}517\ (1)$, $c' = 7{\cdot}858\ (2)$ Å.
Overall temperature factor, $U = 0{\cdot}0095$.
Occupancy factor of 0·5 for Th (see text).

| Atom | Site | Coordinates | |
|---|---|---|---|
| Th | 2(*e*) | $\frac{1}{4}y0$ | $y = 0{\cdot}2437\ (5)$ |
| Nb | 4(*k*) | $\frac{1}{4}yz$ | $y = \frac{3}{4}$, $z = \frac{1}{4}$ |
| O(1) | 2(*e*) | $\frac{1}{4}y0$ | $y = 0{\cdot}844\ (8)$ |
| O(2) | 2(*f*) | $\frac{1}{4}y\frac{1}{2}$ | $y = 0{\cdot}688\ (8)$ |
| O(3) | 4(*h*) | $0\frac{1}{2}z$ | $z = 0{\cdot}226\ (3)$ |
| O(4) | 4(*g*) | $00z$ | $z = 0{\cdot}273\ (3)$ |

| *h k l* | $F_o$ | $F_c$† | *h k l* | $F_o$ | $F_c$ | *h k l* | $F_o$ | $F_c$ |
|---|---|---|---|---|---|---|---|---|
| 0 1 1 | * | 10·7 | 0 3 7 | * | 1·0 | 2 3 0 | * | 10·9 |
| 0 1 2 | * | 6·8 | 0 5 0 | * | 9·2 | 2 3 1 | 21·2 | 21·8 |
| 0 1 3 | 41·1 | 38·7 | 0 5 1 | 14·3 | 16·0 | 2 3 2 | * | 10·6 |
| 0 1 4 | * | 5·6 | 0 5 2 | * | 9·1 | 2 3 3 | 38·4 | 34·4 |
| 0 1 5 | * | 11·4 | 0 5 3 | 31·3 | 25·6 | 2 3 4 | * | 9·9 |
| 0 1 6 | * | 3·8 | 0 5 4 | * | 9·0 | 2 3 5 | * | 5·2 |
| 0 1 7 | 25·3 | 26·0 | 0 5 5 | * | 5·6 | 2 3 6 | * | 8·5 |
| 0 3 0 | * | 10·9 | 2 1 1 | 30·6 | 27·7 | 2 3 7 | 23·4 | 27·4 |
| 0 3 1 | 35·9 | 35·8 | 2 1 2 | * | 7·3 | 2 5 0 | * | 9·9 |
| 0 3 2 | * | 10·4 | 2 1 3 | 18·9 | 11·0 | 2 5 1 | 23·4 | 20·5 |
| 0 3 3 | * | 11·2 | 2 1 4 | * | 6·3 | 2 5 2 | * | 9·8 |
| 0 3 4 | * | 9·2 | 2 1 5 | 26·8 | 28·9 | 2 5 3 | * | 9·8 |
| 0 3 5 | 31·9 | 36·0 | 2 1 6 | * | 5·8 | 2 5 4 | * | 9·4 |
| 0 3 6 | * | 8·4 | 2 1 7 | * | 9·4 | 2 5 5 | 25·4 | 24·2 |

* Unobserved.
† $F_c = [F(hkl)^2 + F(khl)^2]^{1/2}$.

$\langle 110\rangle_p$ columns of thorium atoms, then the pseudocubic subcell axes remain orthogonal as experimentally observed. The factor controlling this interdependence of the octahedral tilts and the lattice expansion due to charge separation is probably the network of microdomain boundaries. To maintain coherence of the oxygen framework across intersecting $(100)_p$ and $(010)_p$ boundaries, the pseudocubic subcell orthogonality (and equality of $a_p$, $b_p$) must be preserved.

### 4.3. *Combined model*

In §§ 4.1 and 4.2 we considered the diffraction effects due to thorium/vacancy ordering and to octahedral tilts (plus small atomic displacements) independently of one another. A complete description of the model for $ThNb_4O_{12}$ should be possible in a unique unit cell and space group. The space group will be within the intersection of the two groups *Immm* and *Pmam*, when they are referred to a common unit cell and a common origin. As a common unit cell we can consider that for the thorium/vacancy ordering, with parameters $a$, $b$, $c$ $(3\sqrt{2}a_p, \sqrt{2}b_p, 4c_p)$, which are simple multiples of those for the cell describing the octahedral tilting, $a'$, $b'$, $c'$ $(\sqrt{2}a_p, \sqrt{2}b_p, 2c_p)$. The $a'$ and $b'$ axes must first be interchanged to ensure that the tilt axes are parallel to the $[\bar{1}10]_p$ columns of thorium atoms and so the space group for the octahedral tilts becomes *Pbmm*. This space group remains invariant with both tripling of $a'$ and doubling of $c'$ so that *Pbmm* is retained in the larger unit cell. However, the origin in *Pbmm* is displaced by $(\frac{1}{4}\frac{1}{4}0)$ relative to that in *Immm*. After effecting the origin shift in *Pbmm*, we find that the equipoints that remain in common to the two space groups are

$$x,y,z; \quad x,\bar{y},\bar{z}; \quad x,\bar{y},z; \quad x,y,\bar{z};$$

these are the equipoints of the space group *P2mm*, which is a maximal nonisomorphic subgroup of *Pbmm*. In principle, a refinement of the complete model for $ThNb_4O_{12}$ in a single-domain approximation should be possible in this space group. We have not attempted this refinement as there are almost three times more positional parameters than the number of observed reflections.

In Fig. 7 we have combined both the octahedral tilts and thorium/vacancy ordering to show (001) sections of the complete model, centered about $z = 0$ and $z = \frac{1}{2}$. The average thorium occupancies are represented by the areas of the filled circles. It is apparent that the statistically most significant contribution to local ordering would comprise $[\bar{1}10]_p$ columns of thoriums, three atoms wide, alternating with equivalent empty columns. The $[\bar{1}10]_p$ columns are further ordered into $(223)_p$ [and $(22\bar{3})_p$] planes; the separation between adjacent columns in these planes is 11·5 Å. For comparison, the separation between adjacent columns in $(001)_p$ planes is 16·5 Å. The distances over which order is established are thus very large, which is consistent with our observations that long-range order is not observed for this compound.

## 5. Discussion

The phase $ThNb_4O_{12}$, when slowly cooled from the melt, displays an interesting hierarchy of ordering patterns. At the top of the ordering scheme is long-range primary ordering of thorium atoms into alternate $(001)_p$ planes of $A$-cation sites. The superlattice reflections which correspond to the doubling of the $c_p$ axis are very sharp; they have the same degree of sharpness as the perovskite subcell reflections. As will

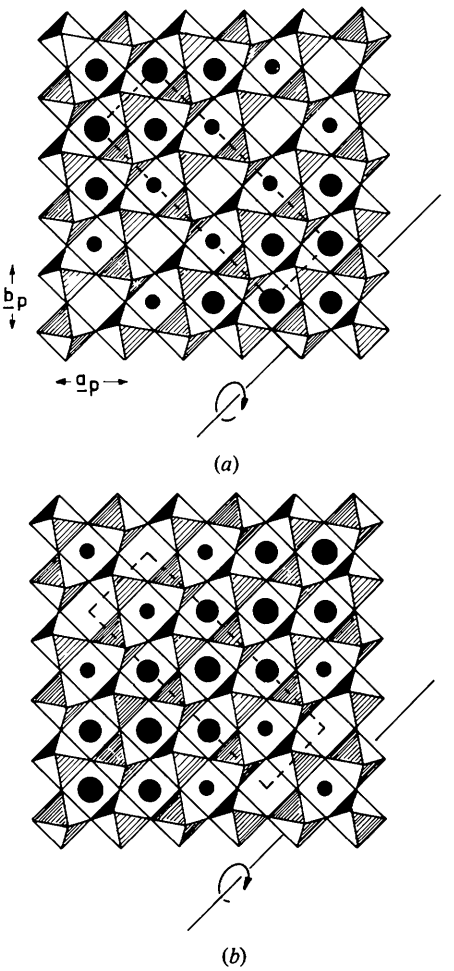


Fig. 7. (001) sections of the model for $ThNb_4O_{12}$ showing both the octahedral tilts and the modulation of thorium scattering density. The area of the filled circles is proportional to the thorium site occupancy. (*a*) and (*b*) represent sections centered at $z = 0$ and $z = \frac{1}{2}$ respectively.

be reported in part II, this primary ordering is well established, even in samples quenched rapidly from the melt. The ordering of the thorium atoms within the $(001)_p$ 'half-occupied' planes is, however, of a very short-range nature. The corresponding diffraction effects are very diffuse and their rod-like nature indicates a lack of long-range correlations *between* $\{110\}_p$ *planes* of thorium atoms. The average correlation length is only 20–30 Å.

*Within* the $\{110\}_p$ planes the *average* ordering periodicities are maintained over distances of the order of hundreds of ångströms. However, presumably due to the difficulty of diffusion of the large, highly charged thorium cations, only an average long-period ordering is observed, which is adequately described by a sinusoidal modulation.

Accompanying the thorium/vacancy density modulation, there is a modulation of atom displacements. The niobium displacements shown in Fig. 6 have been quite accurately established from the structure refinement. In general there is a displacement of all niobium atoms *away* from the occupied thorium sites towards the empty channels, *i.e.* there is an attempt by the niobium cations to balance the highly anisotropic charge distribution formed by the clustering of the tetravalent thorium cations into columns. The displacements are maximum for the niobiums which are associated with the highest density of thoriums (see Fig. 6), *i.e.* the amplitudes of the niobium displacements follow the same modulation pattern as the thorium density modulation. The maximum niobium displacements are about 0·25 Å, which are considerably larger than those observed in perovskites such as $NaNbO_3$ and $KNbO_3$ (Megaw, 1968).

Finally, in the ordering hierarchy, we have an ordered series of oxygen displacements which corresponds to a tilting of the octahedral framework about $\langle 110\rangle_p$ axes, parallel to the columns of thorium atoms. The angle of tilt is about 8°, individual oxygen displacements are in the range 0·2–0·5 Å. The tilts are accompanied by displacements of thorium atoms perpendicular to the $[1\bar{1}0]_p$ columns, see Table 1.

The hierarchy of ordering patterns and the associated correlation lengths are directly related to the formation of microdomains, with domain boundaries parallel to $(100)_p$ and $(010)_p$ and average widths of 25 Å. The description of the microdomain model for $ThNb_4O_{12}$ will be given in a subsequent publication (part II).

We thank the Instituto de Química Inorgánica 'ELHUYAR', CSIC, Spain, for allowing us to use their electron microscopy facilities.

### References

BURBANK, R. D. (1970). *J. Appl. Cryst.* **3**, 112–120.
GLAZER, A. M. (1972). *Acta Cryst.* B**28**, 3384–3392.
KELLER, C. (1965). *J. Inorg. Nucl. Chem.* **27**, 1233–1246.
KOVBA, L. M. & TRUNOV, V. K. (1962). *Dokl. Akad. Nauk SSSR*, **147**, 622–624.
LABEAU, M. & JOUBERT, J. C. (1978). *J. Solid State Chem.* **25**, 347–353.
MEGAW, H. D. (1968). *Acta Cryst.* A**24**, 589.
OGAWA, S. (1962). *J. Phys. Soc. Jpn*, **17**, Suppl. BII, 253–262.
TRUNOV, V. K. & KOVBA, L. M. (1966). *Zh. Strukt. Khim.* **7**, 896–897.

*Acta Cryst.* (1982). A**38**, 186–194

# α-Bungarotoxin Structure Revealed by a Rapid Method for Averaging Electron Density of Non-crystallographically Translationally Related Molecules

BY DAVID A. AGARD AND ROBERT M. STROUD*

*University of California at San Francisco, Department of Biochemistry and Biophysics, School of Medicine, San Francisco, California* 94143, *USA*

(*Received* 7 *November* 1980; *accepted* 11 *June* 1981)

### Abstract

In macromolecular crystallography multiple and independent images of the same chemical species are often present in the crystallographic asymmetric unit. Averaging of density for non-crystallographically related molecules is a powerful technique both for improvement of the density image, and for subsequent phase refinement. Surprisingly often, a non-crystallographic axis of symmetry lies parallel to a crystallographic axis. In such cases, the averaged electron density map can be computed simply and directly from

* To whom reprint requests should be sent.

0567-7394/82/020186-09$01.00 